QUANTUM OPTICS

Logical states for fault-tolerant quantum computation with propagating light

Shunya Konno[1]†, Warit Asavanant[1,2]*, Fumiya Hanamura[1], Hironari Nagayoshi[1], Kosuke Fukui[1], Atsushi Sakaguchi[2], Ryuhoh Ide[1], Fumihiro China[3], Masahiro Yabuno[3], Shigehito Miki[3,4], Hirotaka Terai[3], Kan Takase[1,2], Mamoru Endo[1,2], Petr Marek[5], Radim Filip[5], Peter van Loock[6], Akira Furusawa[1,2]*

To harness the potential of a quantum computer, quantum information must be protected against error by encoding it into a logical state that is suitable for quantum error correction. The Gottesman-Kitaev-Preskill (GKP) qubit is a promising candidate because the required multiqubit operations are readily available at optical frequency. To date, however, GKP qubits have been demonstrated only at mechanical and microwave frequencies. We realized a GKP state in propagating light at telecommunication wavelength and verified it through homodyne measurements without loss corrections. The generation is based on interference of cat states, followed by homodyne measurements. Our final states exhibit nonclassicality and non-Gaussianity, including the trident shape of faint instances of GKP states. Improvements toward brighter, multipeaked GKP qubits will be the basis for quantum computation with light.

Quantum computers whose operations are based on quantum mechanics outperform classical computers in certain tasks, with recent demonstrations of quantum advantage being reported (*1*, *2*). Within a few years, noisy intermediate-scale quantum computers are expected to be available. To go beyond that, however, fault-tolerant quantum processors are required. To mitigate the errors in quantum computation, quantum error correction (QEC) is a promising strategy. QEC allows the detection and correction of errors without disturbing the quantum information by having additional redundancy in the system. QEC that uses bosonic systems has attracted attention owing to their large Hilbert spaces, which are capable of redundantly encoding qubits, and various bosonic codes such as binomial codes (*3*), cat codes (*4*), and Gottesman-Kitaev-Preskill (GKP) codes (*5*) are being explored.

In terms of wave functions, GKP states have a periodic sharp-peaked grid structure in both of their quadratures, which allows for the detection and correction of small loss and displacement errors that are dominant in the optical systems. Advantageously, the basic qubit-level operations on the GKP codes (also called Clifford operations), including entangling gates and error syndrome measurements, can be done using only linear operations. Moreover, universal quantum computation can be achieved by additional light squeezers (*6*), which have been already demonstrated in optical systems, and specifically designed GKP qubit states (*7*, *8*). The key technologies for fault-tolerant quantum computation using GKP qubits are based on quantum teleportation (*9*). Quantum teleportation provides the capability for linear operations with Bell measurement and feedforward displacement that correspond to syndrome measurement and recovery operation, respectively (*10*, *11*). Quantum teleportation technology is highly developed in the optical system (*12*, *13*), which makes it a promising platform for GKP states. The experimental demonstrations of the GKP qubits to date, however, are in stationary systems that can be coupled to qubits (*14*, *15*) providing strong nonlinearity. Conversely, linear operations are not naturally available and have to be constructed by engineering the nonlinearity of the system (*16*, *17*), which limits the scalability to a large-scale multimode interaction. This is in contrast to the optical system, in which linear operations can be simply done with commercially available beamsplitters and multimode linear operations can be easily implemented (*18*, *19*).

In addition to the linearity of the system, there are a few key properties required for the GKP states to be useful in actual quantum computation. The physical platform for using GKP states should allow large-scale and fast operations, because slow implementation of syndrome measurements and corrections increases the error rates and thus entails an additional overhead. Moreover, for applications such as quantum communication or interconnecting quantum computers using quantum internet, GKP states encoded in a propagating wave can be the core elements. Given this, a propagating electromagnetic wave system in the optical regime is a promising candidate. By multiplexing of degrees of freedom such as time (*20*, *21*) or frequency (*22*) in the propagating wave, a large-scale quantum computation platform has already been demonstrated. Also, terahertz-bandwidth light source (*23*), 43-GHz optical homodyne measurement (*24*), and high-speed nonlinear feedforward (*25*), which are key components to high-speed optical quantum computation and error correction, have been demonstrated; this means that we can expect near-term optical quantum computation with a clock frequency of at least a few gigahertz, which surpasses other physical systems by several orders of magnitude. Despite these appealing features, however, the actual optical generation of GKP qubits in a propagating optical system has remained elusive because propagating electromagnetic systems lack viable strong nonlinearity, and even if we try to obtain nonlinearity by using a system such as cavity QED (*26*), a complex arrangement would be required to realize a complex quantum state. By realizing GKP states in the optical system, we can overcome the limitations of multimode linear operations and scalability of the GKP approach in the nonlinear systems (*14*, *15*). Therefore, the realization of GKP states in the propagating wave is a key to practical quantum computation and is the final main ingredient of the fault-tolerant universal quantum computer using optical systems.

There are many research articles and proposals on how to generate optical GKP states [for example, see (*27*–*30*)]. Our method uses some of these concepts and generates the GKP state in a propagating wave system based on the two-mode interference between cat states and a single-mode projection obtained through an optical homodyne measurement (*28*, *29*). This method benefits from the fact that cat states are fairly well known and are experimentally accessible in the optical system (*31*). The required nonlinearity in the GKP state generation is introduced off-line by photon number measurements used in the generation of the cat states. The generated state is characterized through homodyne measurements and is reconstructed with quantum tomography. No corrections for experimental imperfection are used in either the homodyne measurements or quantum tomography. Homodyne measurement is a linear measurement that is required in the syndrome measurements and operations of GKP states. Homodyne measurement of the GKP states, however, has not been implemented in previous experimental demonstrations (*14*, *15*). Although the cat-state generation in this work is probabilistic, given the combination of the cutting-edge photon-number resolving detector (*32*) and methods for high-rate cat-state generation (*33*), the whole process can have a high success rate. Also, for a more complex multistep generation, feedforward displacement based

[1]Department of Applied Physics, School of Engineering, The University of Tokyo, 7-3-1 Hongo, Bunkyo-ku, Tokyo 113-8656, Japan. [2]Optical Quantum Computing Research Team, RIKEN Center for Quantum Computing, 2-1 Hirosawa, Wako, Saitama 351-0198, Japan. [3]Advanced ICR Research Institute, National Institute of Information and Communications Technology, 588-2 Iwaoka, Nishi, Kobe 651-2492, Japan. [4]Graduate School of Engineering, Kobe University, 1-1 Rokko-dai, Nada, Kobe 657-0013, Japan. [5]Department of Optics, Palacky University, 17. listopadu 1192/12, 77146 Olomouc, Czech Republic. [6]Institute of Physics, Johannes-Gutenberg University of Mainz, Staudingerweg 7, 55128 Mainz, Germany.
***Corresponding author. Email: warit@alice.t.u-tokyo.ac.jp (W.A.); akiraf@ap.t.u-tokyo.ac.jp (A.F.)**
†Present address: NTT Device Technology Laboratories, NTT Corporation, Atsugi-shi, Kanagawa 243-0198, Japan.

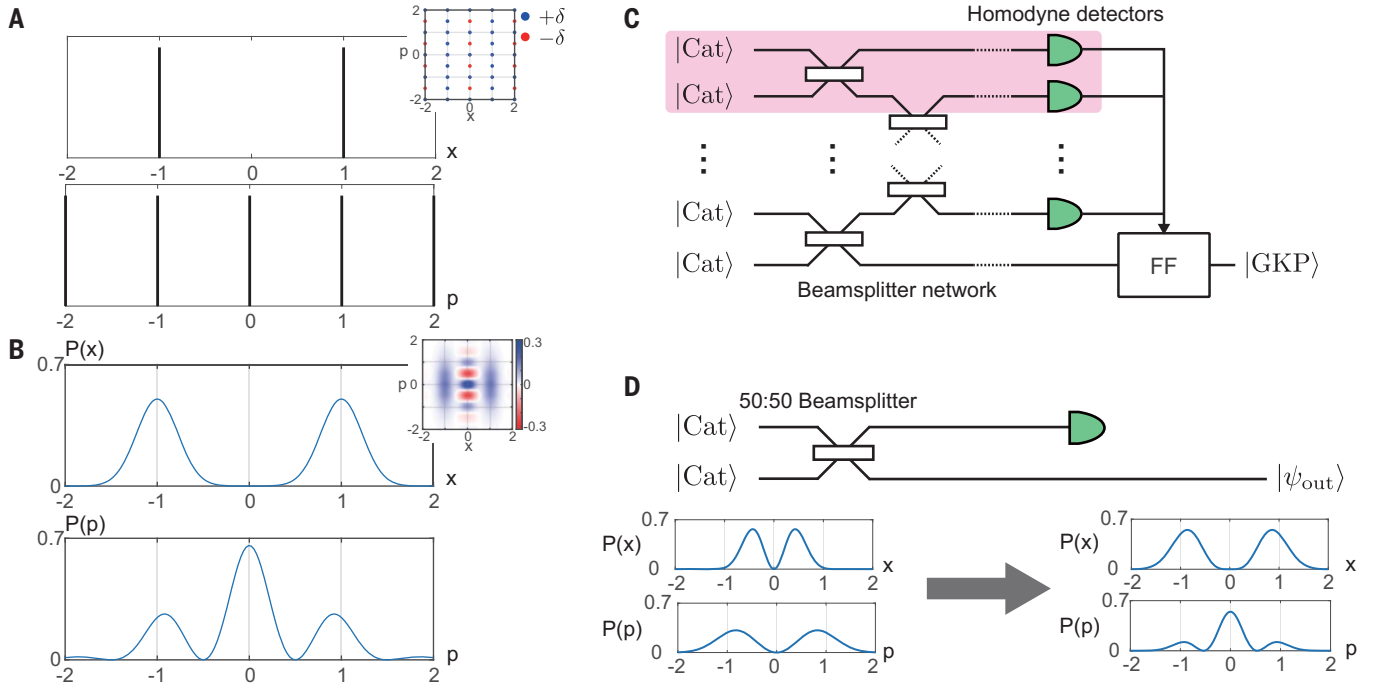

Fig. 1. GKP state and its generation method in the optical system. (**A** and **B**) Quadrature distributions of ideal (infinite energy) (A) and approximated GKP |1⟩ states (B) with 5 dB of squeezing (the units are defined with reduced Planck's constant $\hbar = 1$, and the quadratures are normalized to $\sqrt{\pi}$). The insets show the Wigner functions. δ, Delta function peak. (**C**) General generation method in the optical system based on the interference of cat states using a beamsplitter network and implementing homodyne measurements and feedforward operations (FFs) that incorporate squeezing and displacement operations. Light red shading indicates the single step of the generation method. (**D**) Single step of the generation method. Note that FFs with Gaussian operations are omitted in this figure and are replaced by conditioning in this experiment. The formation of peaks at the stabilizer values is visible.

on the results of the homodyne measurements can be done to remove the need for the homodyne conditioning (*29*), which makes the process after cat-state generation semideterministic.

GKP state and generation methodology

The GKP state can be defined in several ways; in this work, we consider a GKP state with square lattice structure. When we consider the basic observables of light—quadrature operators $\hat{x}$ and $\hat{p}$ ($[\hat{x}, \hat{p}] = i$)—the Pauli operators on the phase-space grid are $\hat{\hat{X}} = \exp(-i\sqrt{\pi}\hat{p})$ and $\hat{\hat{Z}} = \exp(i\sqrt{\pi}\hat{x})$, which correspond to displacement in x and p by $\sqrt{\pi}$, respectively. Then, the GKP states are defined in the logical space that is stabilized, that is, invariant, under the operators $\hat{S}_x = \hat{\hat{X}}^2 = \exp(-i2\sqrt{\pi}\hat{p})$ and $\hat{S}_p = \hat{\hat{Z}}^2 = \exp(i2\sqrt{\pi}\hat{x})$, which are displacements by $2\sqrt{\pi}$ in the x and p directions, respectively (*5*). Alternatively, for any ideal GKP states in the logical space, we have $\langle \hat{S}_x \rangle = \langle \hat{S}_p \rangle = 1$. This means that ideal GKP states should have periodicity of $2\sqrt{\pi}$ in both x and p. Defining these two stabilizers does not uniquely determine the states; they determine a logical space in which the information is encoded, and we have to consider another stabilizer to define our state. We can define our basis for the logical space, that is, the eigenstates for $\hat{\hat{Z}}$, as $|0_L\rangle \propto \sum_k |x = 2k\sqrt{\pi}\rangle$ and $|1_L\rangle \propto \sum_k |x = (2k+1)\sqrt{\pi}\rangle$, where the sum k is over all integers. These two states have $\hat{\hat{Z}}$ and $-\hat{\hat{Z}}$ as their stabilizers, respectively, making one of the two GKP code stabilizers $\hat{S}_p$ redundant. Note that $\pm\hat{\hat{Z}}$ commutes with both $\hat{S}_x$ and $\hat{S}_p$. Because these states are unnormalizable, they are usually approximated by replacing the position eigenstates with squeezed states, and the whole states are enveloped with a Gaussian envelope for the symmetry in both the x and p quadrature (*34*). Figure 1, A and B, shows the grid quadrature distribution of an ideal and approximated GKP state.

We generated the peak structure of the GKP states by using the interference of kitten states and homodyne measurements (*28*, *29*). Figure 1C shows a diagram of the general generation method. As an example, let us consider a single interference step (shown in Fig. 1D). If we interfere two cat states $|\psi_{cat}\rangle \propto |i\alpha\rangle - |-i\alpha\rangle$, where $|i\alpha\rangle$ and $|-i\alpha\rangle$ are coherent states with α being a real number, the output two-mode state is $(|i\sqrt{2}\alpha\rangle + |-i\sqrt{2}\alpha\rangle)|0\rangle - |0\rangle(|-i\sqrt{2}\alpha\rangle + |i\sqrt{2}\alpha\rangle)$. If we measure the first mode and condition it at $x = 0$, we will approach $|\psi_{out}\rangle \propto |-i\sqrt{2}\alpha\rangle - 2|0\rangle + |i\sqrt{2}\alpha\rangle$. The output state now approaches the central part of the GKP state in the phase space (up to additional squeezing), and the process can be repeated so that a larger part of the GKP state is synthesized. The coefficients of the peaks in this method can be easily shown to be binomial coefficients that approach Gaussian distribution for a large number of peaks (*28*). To make the width of the peaks small and the distance between the peaks correct as a GKP state, one can either implement the squeezing operation at the end or start with squeezed cat states instead of an unsqueezed cat state (*28*, *29*). Such Gaussian operations only shape the GKP state and do not increase the non-Gaussian grid aspects. Although we use ordinary cat states for our experimental demonstration, squeezing operations on a cat state (*6*) and the high-rate generation of squeezed cat states (*33*) are both being explored in optics.

Experimental results

Figure 2 shows the experimental system. The master laser of the system is a continuous-wave laser with a wavelength of 1545.32 nm and a second-harmonic generator for the generation of 772.66-nm light. The kitten states for the interference are generated by using photon subtraction on squeezed light (*35*). The squeezed light sources are optical parametric oscillators (OPOs). We detected the photon in the photon subtraction using superconducting nanostrip single-photon detectors (SNSPDs). The coincidence detection at both SNSPDs heralded success in the interference. We measured one of the

modes in the x basis using a homodyne detector so that the GKP state was generated in the other mode. The signal of the SNSPDs acted as the measurement trigger for the oscilloscope, and the electrical signals of the homodyne detectors were measured in real time. We measured the quadrature of the other mode at various phases and used the collected data to reconstruct the state by quantum tomography. No correction for optical losses or any experimental imperfections were done on the measurement results or during the tomography process. Note that in this work, we only implemented a single step, and iterations need to be done in the future to realize high-quality GKP states (*28*, *29*). Also, we replaced the additional displacement operation for correcting the effects of homodyne measurement with conditioning of the homodyne measurement outcomes. See fig. S1 for details on the experimental systems (*36*).

For GKP states to be useful, they must be able to detect and correct the error displacement in both the x and p quadratures. Although it is prohibited by the uncertainty principle for both quadratures to be sharply defined, locally we can have a Wigner function with sharp peaks. If we consider the Wigner function in Fig. 3 and consider the center positive peak, where all nearby positive regions are considered as a part of the peak, the variances in each quadrature are $\langle\Delta^2\hat{x}\rangle$=1.45±0.03, $\langle\Delta^2\hat{p}\rangle$ = 0.070±0.001, and $\langle\Delta^2\hat{x}\rangle\langle\Delta^2\hat{p}\rangle$ = 0.100±0.002, which is well within the sub-Planck regime (*37*) ($\langle\Delta^2\hat{x}\rangle\langle\Delta^2\hat{p}\rangle < 0.25$). A sub-Planck regime that occurs simultaneously in both quadratures is a regime that cannot be reached

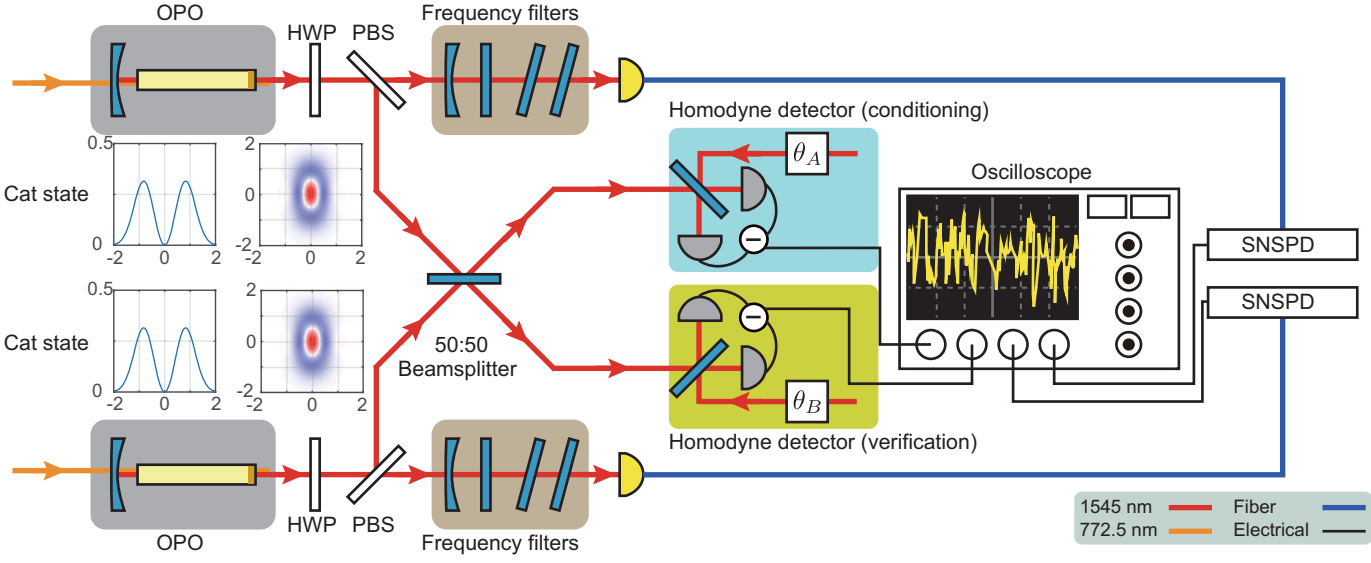

Fig. 2. Experimental setup. Schematic of the experimental setup used in this work. The insets show the ideal states from the photon subtraction with the quadrature distribution in p. The phases of the two homodyne measurements are given by θ_A and θ_B, where θ_A is set to 0° for measuring and conditioning of x quadrature and θ_B is set to 0°, 30°, 60°, 90°, 120°, or 150° for collecting quadrature values for quantum tomography. HWP, half-wave plate; PBS, polarization beamsplitter.

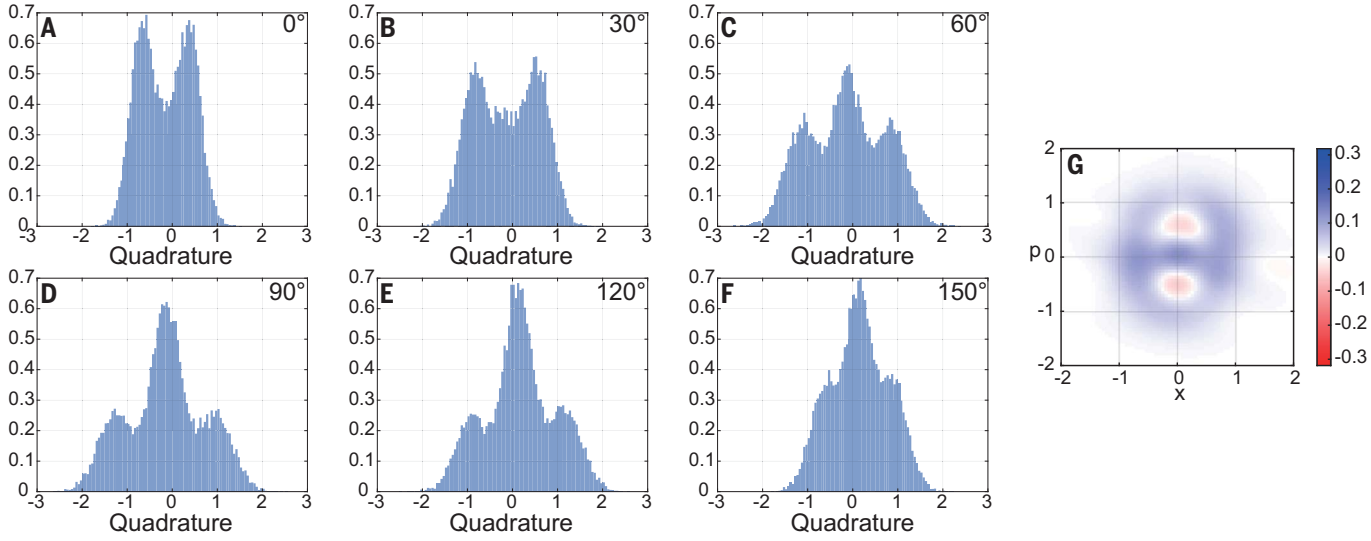

Fig. 3. Quadrature distributions and reconstructed Wigner function. The experimentally measured quadrature distributions are normalized as a probability density function. No corrections were performed on the obtained distributions. (**A** to **F**) Quadrature distributions of the generated states. The homodyne phases are provided in each panel. (**G**) The reconstructed Wigner function. The Gaussian corrections, which correspond to a linear symplectic transformation in phase space, are implemented on the reconstructed Wigner function [see (*36*)]. The color scale bar indicates the values of Wigner function.

with a simple Gaussian state, and this sub-Planck structure is qualitative evidence that our approach can synthesize the sharp delta-function peak structure of the GKP state. Note that the value $\langle \Delta^2 \hat{x} \rangle$ is limited by the amplitude of the initial kitten state and can be improved by using a cat state with a bigger amplitude.

Regarding the quantitative evaluation, we assessed the stabilizers of the generated state. As we mentioned, for our specific state $|1_L\rangle$, the two stabilizers become $\hat{S}_x$ and $\hat{S}_{|1\rangle} = -\hat{Z}$. We calculated the average value of the stabilizers from the generated states, and they are $\langle \hat{S}_x \rangle$=0.170±0.003 and $\langle \hat{S}_{|1\rangle} \rangle = 0.216 \pm 0.006$, respectively. Although these values are still far from unity, they clearly surpass the values that can be achieved with classical states. Furthermore, their collective properties overcome the limits set by Gaussian states. See the supplementary materials for a more detailed analysis and discussion.

Conclusions and discussion

The effective squeezing of our optical GKP state is estimated to be about 2.5 dB, which is, at present, lower than those reported in the trapped ion (5.5 and 7.3 dB) (*14*) and microwave (between 7.4 and 9.5 dB) (*15*). Presently, the limiting factor is the optical loss in the system and the lack of iteration in our demonstration. The mode mismatch between two OPOs is also a relevant source of imperfection, but it can be removed by properly tailoring the temporal mode (*36*). In addition, we also need to make a cat state with larger amplitude and concatenate the process with deeper circuit depth, as depicted in Fig. 1, to increase this effective squeezing. The generalized photon subtraction (*33*) is a promising approach for this because the generated cat states are squeezed and the success rate can be three to six orders of magnitude greater than that of the conventional method. Furthermore, it is possible to use the time-domain multiplexing technique to increase the circuit depth in a hardware-efficient way (*31*). Our present setup has a success rate of about 10 Hz, which is as expected from the experimental parameters (*36*). In addition to the aforementioned generalized photon subtraction, improving the squeezed light source and the photon-number resolving detector can increase the success rate. Regarding the former, improvement can be achieved by replacing the OPO in this work with a terahertz-bandwidth optical parametric amplifier (*23*). Regarding the latter, although the photon counter in this experiment is based on SNSPDs without photon-number resolution, with proper technique, SNSPDs can be used for counting photons with high speed (timing jitter of ~20 ps) (*38*). Using these SNSPDs would allow an even higher generation rate of the cat state for GKP-state generation.

Finally, we briefly comment on how optical GKP states generated in the manner described in this work can be used in actual quantum computation. Because the GKP states generated by this method are a propagating wave, they can be coupled into the various types of optical quantum processors seamlessly without requiring any additional processes such as wavelength conversion. Multimode linear operations (*18*, *19*), quantum teleportation (*12*, *13*), and squeezing operation (*6*) on a propagating optical field have already been demonstrated and implemented, and these technologies can be used to implement syndrome measurement and recovery operations on a GKP state.

REFERENCES AND NOTES

1. H. Wang *et al*., *Phys. Rev. Lett.* **123**, 250503 (2019).
2. H.-S. Zhong *et al*., *Science* **370**, 1460–1463 (2020).
3. M. H. Michael *et al*., *Phys. Rev. X* **6**, 031006 (2016).
4. P. T. Cochrane, G. J. Milburn, W. J. Munro, *Phys. Rev. A* **59**, 2631–2634 (1999).
5. D. Gottesman, A. Kitaev, J. Preskill, *Phys. Rev. A* **64**, 012310 (2001).
6. Y. Miwa *et al*., *Phys. Rev. Lett.* **113**, 013601 (2014).
7. S. Konno *et al*., *Phys. Rev. Res.* **3**, 043026 (2021).
8. B. Q. Baragiola, G. Pantaleoni, R. N. Alexander, A. Karanjai, N. C. Menicucci, *Phys. Rev. Lett.* **123**, 200502 (2019).
9. N. C. Menicucci, *Phys. Rev. Lett.* **112**, 120504 (2014).
10. B. W. Walshe, R. N. Alexander, N. C. Menicucci, B. Q. Baragiola, *Phys. Rev. A* **104**, 062427 (2021).
11. W. Asavanant, K. Fukui, A. Sakaguchi, A. Furusawa, *Phys. Rev. A* **107**, 032412 (2023).
12. A. Furusawa *et al*., *Science* **282**, 706–709 (1998).
13. N. Lee *et al*., *Science* **332**, 330–333 (2011).
14. C. Flühmann *et al*., *Nature* **566**, 513–517 (2019).
15. P. Campagne-Ibarcq *et al*., *Nature* **584**, 368–372 (2020).
16. Y. Y. Gao *et al*., *Nature* **566**, 509–512 (2019).
17. X. Pan *et al*., *Phys. Rev. X* **13**, 021004 (2023).
18. W. Asavanant *et al*., *Phys. Rev. Appl.* **16**, 034005 (2021).
19. M. V. Larsen, X. Guo, C. R. Breum, J. S. Neergaard-Nielsen, U. L. Andersen, *Nat. Phys.* **17**, 1018–1023 (2021).
20. W. Asavanant *et al*., *Science* **366**, 373–376 (2019).
21. M. V. Larsen, X. Guo, C. R. Breum, J. S. Neergaard-Nielsen, U. L. Andersen, *Science* **366**, 369–372 (2019).
22. O. Pfister, *J. Phys. At. Mol. Opt. Phys.* **53**, 012001 (2019).
23. T. Kashiwazaki *et al*., *Appl. Phys. Lett.* **119**, 251104 (2021).
24. A. Inoue *et al*., *Appl. Phys. Lett.* **122**, 104001 (2023).
25. A. Sakaguchi *et al*., *Nat. Commun.* **14**, 3817 (2023).
26. V. Magro, J. Vaneecloo, S. Garcia, A. Ourjoumtsev, *Nat. Photonics* **17**, 688–693 (2023).
27. I. Tzitrin, J. E. Bourassa, N. C. Menicucci, K. K. Sabapathy, *Phys. Rev. A* **101**, 032315 (2020).
28. H. M. Vasconcelos, L. Sanz, S. Glancy, *Opt. Lett.* **35**, 3261–3263 (2010).
29. D. J. Weigand, B. M. Terhal, *Phys. Rev. A* **97**, 022341 (2018).
30. K. Fukui *et al*., *Phys. Rev. Lett.* **128**, 240503 (2022).
31. W. Asavanant, A. Furusawa, *Optical Quantum Computers: A Route to Practical Continuous Variable Quantum Information Processing* (AIP Publishing LLC, 2023).
32. M. Endo *et al*., *Opt. Express* **31**, 12865–12879 (2023).
33. K. Takase, J. Yoshikawa, W. Asavanant, M. Endo, A. Furusawa, *Phys. Rev. A* **103**, 013710 (2021).
34. T. Matsuura, H. Yamasaki, M. Koashi, *Phys. Rev. A* **102**, 032408 (2020).
35. M. Dakna, T. Anhut, T. Opatrný, L. Knöll, D.-G. Welsch, *Phys. Rev. A* **55**, 3184–3194 (1997).
36. See supplementary materials.
37. W. H. Zurek, *Nature* **412**, 712–717 (2001).
38. M. Endo *et al*., *Opt. Express* **29**, 11728–11738 (2021).
39. S. Konno *et al*., Propagating Gottesman-Kitaev-Preskill states encoded in an optical oscillator. Dryad (2023); https://doi.org/10.5061/dryad.t76hdr86j.

ACKNOWLEDGMENTS

Funding: This work was partly supported by the Japan Science and Technology (JST) Agency (Moonshot R&D) grants JPMJMS2064 and JPMJMS2066; by the UTokyo Foundation; and by donations from the Nichia Corporation of Japan. S.K. acknowledges funding from the Japan Society for the Promotion of Science (JSPS) KAKENHI (no. 21J11615). W.A. acknowledges funding from JSPS KAKENHI (no. 23K13040). M.E. acknowledges funding from JST (JPMJPR2254). W.A. and M.E. acknowledge support from the Research Foundation for OptoScience and Technology. P.v.L. acknowledges funding from the Federal Ministry of Education and Research (BMBF) in Germany (QR.X, PhotonQ, and QuKuK) the Deutsche Forschungsgemeinschaft (DFG, German Research Foundation) – Project-ID 429529648 – TRR 306 QuCoLiMa ("Quantum Cooperativity of Light and Matter"), from the European Union and BMBF through QuantERA (ShoQC), and from the European Union's HORIZON Research and Innovation Actions (CLUSTEC). P.M. acknowledges support from grant no. 22-08772S of the Czech Science Foundation (GACR) and the European Union's HORIZON Research and Innovation Actions under grant agreement no. 101080173 (CLUSTEC). R.F. acknowledges project 21-13265X of the Czech Science Foundation. P.M. and R.F. acknowledge EU H2020-WIDESPREAD-2020-5 project NONGAUSS (951737) under the Coordination and Support Action (CSA). **Author contributions:** S.K. led the experiment with supervision from W.A., K.T., M.E., and A.F. S.K. collected the experimental data. S.K. and W.A. analyzed the data. W.A. visualized the data for the manuscript. Theoretical discussions and interpretations of the data were done by W.A., P.v.L., R.F., P.M., F.H., H.N., K.F., A.S., and R.I. The criteria in the supplementary materials was developed by P.M., W.A., and R.F. H.T., S.M., M.Y., and F.C. provided the SNSPDs that were used in this experiment. W.A. wrote the manuscript and the supplementary materials with the help of P.v.L., A.F., P.M., R.F., and the other authors. **Competing interests:** The authors declare no competing interests. **Data and materials availability:** The quadrature obtained and used in this paper is available at Dryad (*39*). Additional data are available in the supplementary materials.

SUPPLEMENTARY MATERIALS

science.org/doi/10.1126/science.adk7560
Materials and Methods
Supplementary Text
Figs. S1 to S4
References (*40*–*44*)

Submitted 8 September 2023; accepted 16 November 2023
10.1126/science.adk7560